Effect of precipitation process parameters on boehmite properties: in situ optical monitoring

Sara Kirchner, Sébastien Teychené, Malika Boualleg, Aurélie Dandeu, Christine Frances, Beatrice Biscans

Effect of precipitation process parameters on boehmite properties: In situ optical monitoring

Sara Kirchner [a,b], Sébastien Teychené [a], Malika Boualleg [b], Aurélie Dandeu [b], Christine Frances [a], Béatrice Biscans [a,*]

[a] Laboratoire de Génie Chimique, UMR CNRS 5503, Université de Toulouse, BP 84234 Campus INP-ENSIACET, 4 allée Émile Monso, 31432 Toulouse Cedex 4, France
[b] IFP Énergies nouvelles, Rond-point de l'échangeur de Solaize, BP 3, 69360 Solaize, France

HIGHLIGHTS

- Boehmite is precipitated either in double-jet stirred tank reactor or micro-mixer.
- Supersaturation would be the major parameter which controls aggregation.
- Multiple light scattering brings out differences during precipitation.

ABSTRACT

Alumina, which is a catalyst support, is obtained by boehmite calcination. This work aims to study boehmite precipitation and the impact of this step on alumina quality. Precipitation of boehmite is studied in a double-jet stirred tank and with a micro-mixer. These devices induce different mixing of the reagents and different evolution of the supersaturation. Precipitation is followed on-line with an optical apparatus based on multiple light scattering. Alumina obtained with micro-mixer presents significantly lower specific surface area, pore volume and mean pore diameter than the one obtained with the double jet reactor, showing a totally different crystallite aggregation. Using different types of micromixers at isosupersaturation, the results show that Reynolds number in the micro-mixer, stirring power in the receiving vessel and micro-mixer type have no effect on porosity and thus on aggregation, which could be explained by a supersaturation that is sufficiently high to prevent other parameters from having effects. Using double jet reactor, feeding time directly affects initial supersaturation, which level is lower than the one created in micro-mixer. For double jet precipitation, the textural properties are directly correlated to the initial supersaturation. Alumina obtained with the highest value of supersaturation with double-jet stirred tank has similar porosity value than the one obtained in micro-mixer. This supersaturation level would thus be a threshold beyond which other operating parameters have no effect. Aggregation would be directly controlled by initial supersaturation. Furthermore, it was shown that differences of alumina textures are correlated with different behaviors of backscattering levels. This technique allows the in situ characterization of aggregation differences, during precipitation, before the impact of filtration–washing–drying steps on aggregation.

Keywords:
Precipitation
Aggregation
Multiple light scattering
Boehmite
Alumina
Micro-mixer

1. Introduction

γ-Alumina is a catalyst support Al_2O_3, used in many refinery processes. This material is obtained from calcination of boehmite AlOOH. Transformation of boehmite to γ-alumina is topotactic [1,2], with the morphological properties of boehmite being largely preserved during the phase change. The control of alumina properties, and therefore of boehmite, is essential to optimize the catalysts.

Various synthesis routes are possible for boehmite. It can be prepared by the sol gel process using aluminum alkoxides [3,4]. However, the synthetic route used industrially involves the precipitation of aluminum salts, which may be followed by a period of ripening in hydrothermal conditions [5–7].

* Corresponding author. Tel.: +33 534323638.
E-mail addresses: sara.kirchner@ensiacet.fr (S. Kirchner), sebastien.teychene@ensiacet.fr (S. Teychené), malika.boualleg@ifpen.fr (M. Boualleg), aurelie.dandeu@ifpen.fr (A. Dandeu), christine.frances@ensiacet.fr (C. Frances), beatrice.biscans@ensiacet.fr (B. Biscans).

http://dx.doi.org/10.1016/j.cej.2015.06.002

Several aluminum salts can be used to obtain boehmite, such as aluminum nitrate, $Al(NO_3)_3$ [8–10], aluminum chloride, $AlCl_3$ [8], or aluminum sulfate, $Al_2(SO_4)_3$ [8,11]. The latter reagent was used in this work. Sulfate ions have huge importance since they direct aggregation. Sulfate ions are bound by hydrogen bonds, in acidic conditions [11], since they have high affinity for aluminum [8]. This adsorption would be selective, on [010] and [001] faces [11]. Thus, the growth of boehmite would occur preferentially on [100] faces, resulting in the formation of fibrillar boehmite [7].

The effects of physicochemical conditions on boehmite precipitation are relatively well known. Temperature and pH are the most influential parameters [9,10,12], and to a lesser extent, the reagents [7,8].

Nevertheless, little work concerns the mechanisms managing crystallites formation and their aggregation, which is the source of the porosity of the material. Rousseaux et al. [13] studied the effect of different precipitators on boehmite particle properties, and, in particular, the effect of operating parameters. These authors show that increasing the intensity of vessel mixing decreases the crystallite size. They also show that using two different technologies of reactors (vortex reactor and sliding surface reactor) and varying the profiles of the suspension circulation inside the reactor, i.e. the way the existing particles go through the reaction zone where fresh reagents are introduced, the porous volume and mean pore diameter change. Another work has shown that using sliding surface mixing device, whose mixing is more efficient than in vortex reactor, gives higher specific surface area, porous volume and mean pore diameter [14]. Effect of mixing on gibbsite precipitation has been studied. Ilievski et al. [15] showed that gibbsite agglomeration is affected by shear rate, which is expected to have an effect on particle capture efficiency. Mixing, which is expected to control collision rates, has not a significant effect on precipitation, in the case of gibbsite.

Another aspect of boehmite precipitation is to obtained in situ data without disturbing the suspension structure by sampling. Recently, direct techniques were developed to characterise on-line and in-line properties of concentrated dispersions in a non-intrusive and non-denaturing way.

Raman spectroscopy [16], which allowed quantifying the impact of mixing rate or seeding parameters [17], chemical imaging [18], FTIR [19] which is a supersaturation sensor, X-ray diffraction [20], FBRM [21] which has given information about the influence of process conditions on the formed material, ultrasonic attenuation spectroscopy [22]. Ultrasonic spectrometry techniques for example, provide advantages for on-line particle size analyses, particularly the ability to operate on undiluted and optically opaque media. The technique consists in propagating ultrasonic waves of variable frequency through the particulate system and measuring the frequency dependence of the attenuation to derive particle size [23–26]. The ultrasonic velocity method and the electroacoustic technique can also be used for particle size characterization in concentrated systems. The ultrasonic velocity method consists in measuring the transit time of pulsed multiple frequency ultrasonic waves propagating through a medium [27]. In the electroacoustic method, an alternating electric field causes the electrically charged particles to move back and forth generating sound waves. Zeta potential and particle size are derived from the analysis of sound waves in relation with particle motions [28].

Multiple light scattering methods represent an alternative to acoustic spectrometry techniques for the characterization of particles flows. In the multiple scattering regime, the transport mean free path representative of particle size indeed can be derived from the analysis of the light flux distribution in the incoherent backscattered spot light [29–31]. In a previous works, the multiple light scattered was analysed from a concentrated dispersion (Turbiscan On Line instrument) during calcium carbonate batch precipitation. Size and mean refractive index of particles or nuclei agglomerates are derived from measurements of the backscattered light flux on the basis of a multiple light scattering model [31,32].

Our study focuses on understanding the impact of precipitation processes and process parameters on the aggregation of boehmite crystallites, and the effect on material quality, by following precipitation with the on-line optical device Turbiscan On Line. In this study, precipitation experiments in double-jet stirred tank reactor and with a pre-mixing device were compared. The effect of the addition time of the whole reactants and of the mixing, on material properties were analyzed.

2. Materials and methods

2.1. Precipitation–reaction

Boehmite is synthesized by mixing an aluminum sulfate solution with a sodium aluminate solution through the heterogeneous reaction:

$$Al_2(SO_4)_{3_{(aq)}} + 6NaAl(OH)_{4_{(aq)}} \rightarrow 8AlOOH_{(s)} + 3Na_2SO_{4_{(aq)}} + 8H_2O \quad (1)$$

All chemicals involved in this synthesis were reagent grade and used as received without further purification. pH was controlled at 9 and temperature was 60 °C.

After synthesis, the suspension was filtered and washed five times with water (T = 60 °C) in order to minimize the content of impurities (Na^+ and SO_4^{2-}). The cake was dried at 120 °C overnight and then ground. Dry boehmite was finally calcined during 4 h at 540 °C in order to obtain γ-alumina (γ-Al_2O_3).

2.2. Precipitation set-up

In this study, experiments were carried out in a 2 L stirred tank reactor with two types of mixing systems: double-jet of the reagents in the stirred tank or pre-mixing of the reagents before introduction in the stirred tank.

2.2.1. Double-jet stirred tank reactor

Aluminum sulfate solution ($Al_2(SO_4)_3$) (C = 0.35 mol/l, V = 175 ml) was introduced simultaneously with a sodium aluminate solution ($NaAl(OH)_4$) (C = 0.99 mol/L, V = 262 ml), over 30 min, in a stirred vessel containing water (660 ml) at constant conditions of temperature and pH (60 °C and pH = 9). Water was also added during precipitation (V = 903 ml). The molar ratio $R = n_{NaAl(OH)_4}/n_{Al_2(SO_4)_3}$ was equal to 4.2. All these conditions were fixed in order to obtain predominantly boehmite (and no gibbsite or other polymorphs). A pH regulation maintained the pH at 9 by controlling a sodium aluminate solution pump (Fig. 1). Suspension was analyzed throughout the precipitation with an on-line optical device (Turbiscan On Line instrument) (see Section 2.3) using a peristaltic pump.

The reactor was a standard cylindrical stirred tank equipped with an 8 cm 4-blade Teflon-coated impeller. Four baffles prevented vortex formation. Mixing parameters are shown in Table 1.

In the stirred tank reactor mixing inhomogeneity due high reagent feed rates and volume variation, results in inhomogeneity of supersaturation, due to gradients of solution [33] and particle concentration [34] and having an effect on primary nucleation [35].

In fact, the variation of supersaturation is due to the progressive addition of the reagents over 30 min, inside the vessel containing a suspension changing spatially because the concentration is not homogeneous in the tank, and temporally, since, according to the progress of the reaction, the particles are formed in an already

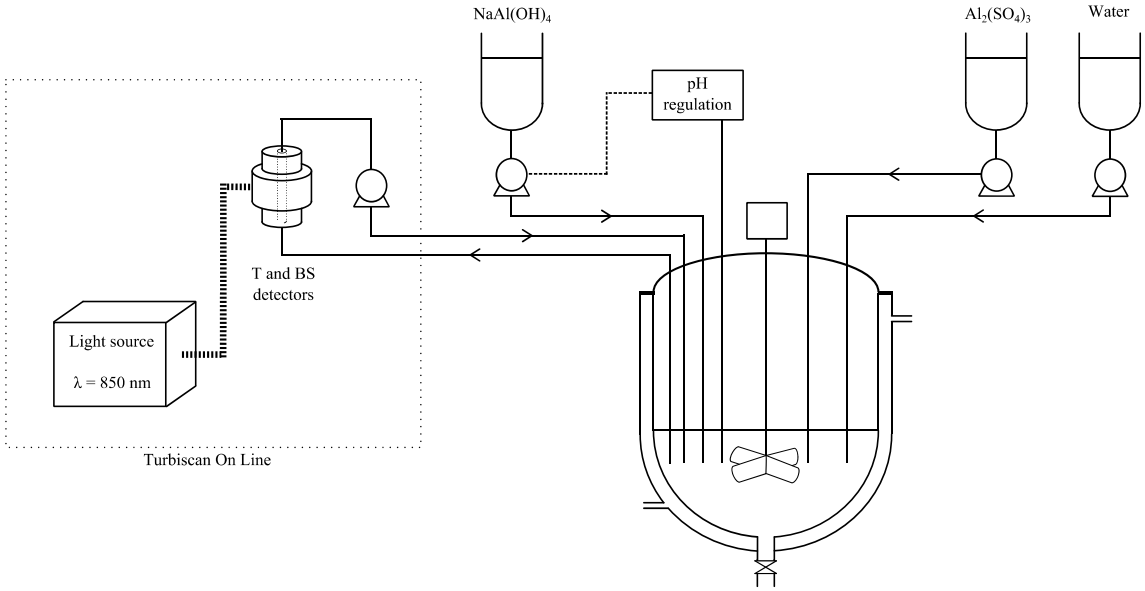

Fig. 1. Double-jet stirred tank device used for boehmite precipitation and Turbiscan On Line apparatus.

Table 1
Mixing characteristics of the double-jet stirred tank and reagents flow rates.

Vessel stirring power (W/m^3)	Vessel Reynolds number	Feeding flow (ml/min)			Reagents addition time (s)
		$NaAl(OH)_4$	$Al_2(SO_4)_3$	Water	
250	52×10^3	8.7	5.8	30.1	1800

more or less concentrated medium. Moreover, in this semi-batch process, particles appeared in a medium already containing particles. Nucleation was therefore of secondary type.

2.2.2. Micro-mixing device

In that configuration, precipitation was performed by using a micro-mixer. Two geometries of micro-mixers, Hartridge–Roughton [36] (HR) and Y, were used in this study.

They both have 2 mm inlet tubes and 4 mm outlet tubes. An angle of 60° separates the Y inlet tubes. Micro-mixing time, t_μ has been determined in the literature for these types of micro-mixers: t_μ (HR) = 1.2 ms and t_μ (Y) = 3.8 ms (1 mm inlet tubes, 2 mm outlet, 90° angle for Y, fluid velocity of 15 m s^{-1} in the central tube) [37]. The HR micro-mixer is therefore the more efficient and was used in the first part of the work.

Using micro-mixers implies some constraints. First, it is necessary to proceed with high enough flow rates in order to prevent the mixer from clogging. In this study, it has been chosen to operate the micro-mixer with equal reagents flow rates because it results in a better micro-mixing efficiency as shown by CFD simulation [38,39]. Another important aspect in our study is that the pH cannot be controlled inside the mixer. The reagent concentrations were adjusted to obtain a pH of 9 in the micro-mixer outlet tube. In addition, to have comparable systems in terms of reagents molar ratio and because the micro-mixers have two inlets, the amount of water added in double-jet stirred tank reactor during precipitation is shared between both reagents. Consequently, the reagents concentrations were 0.92 mol/l for $NaAl(OH)_4$ and 0.24 mol/l for $Al_2(SO_4)_3$.

Precipitation is performed by injecting both reagents heated at 60 °C during 90 s to reach the same boehmite concentration as in the case of double-jet precipitation. The product formed at the outlet of the micro-mixer is then poured in a crystallizer initially filled with 666 ml of water heated at 60 °C.

The total precipitation time was 30 min, including the reagent addition phase and suspension ripening phase at a controlled temperature. During the ripening phase, controlled addition of sodium hydroxide allows to kept the constant value of pH at 9. The downstream processes were the same as in Section 2.2.1.

Mixing parameters are presented in Table 2. The micro-mixer Reynolds number is calculated considering the outlet tube dimension and the viscosity of water at 50 °C (5.56×10^{-7} m^2 s^{-1}). Micro-mixer residence time is the time that the one taken for the suspension to move through the outlet tube.

The micro-mixing step is the major difference when using the double-jet stirred tank or the micro-mixing device and this affects supersaturation level. Considering reagents with equivalent concentrations in both experiments, the level of supersaturation is much higher in the micro-mixing device, where reagents meet directly, than in a double-jet stirred tank where reagents meet in water and are then diluted.

Otherwise, particles appear in a medium with constant supersaturation in micro-mixers, whereas supersaturation is not spatially and temporally constant in double-jet stirred tank precipitation. Moreover, in micro-mixers, spontaneous precipitation occurs since the medium does not contain particles beforehand. In double-jet stirred tank precipitation, particles appear in a medium already containing particles. Accordingly, residence time in the vessel is almost the same for all particles using a micro-mixer, whereas it is different in double-jet stirred tank devices (from 0 to 30 min).

2.3. On-line characterization: multiple light scattering

The Turbiscan On Line device, based on multiple light scattering [32], is used to follow precipitation with the two devices. This technique used for precipitation and crystallization processes enable to determine a characteristic size from low concentration suspension

Table 2
Mixing characteristics of micro-mixer device and reagent flow rates.

Vessel stirring power (W/m^3)	Vessel Reynolds number	Feeding flow (ml/min)		Micro-mixer Reynolds number	Reagents addition time (s)	Micro-mixer residence time (s)
		$NaAl(OH)_4$	$Al_2(SO_4)_3$			
250	52×10^3	430	430	8×10^3	92	2.6×10^{-2}

to highly concentrated disperse media. Using the theoretical development performed in previous works [31], measurement of the transmission level *TR* (Λ) and of the backscattering level) *BS* (Λ^*) of the suspension by Turbiscan on line device, allow determination of the photon mean path Λ and transport mean path Λ^*. Using the Mie theory, Sauter diameter of particles l can be estimated by knowing the particle volume fraction ϕ. Alternatively, ϕ can be calculated by knowing l.

The backscattering value obtain with this technique is the ratio between the intensity measured and a reference intensity. Fig. 2 shows the theoretical evolution of backscattering level as a function of the diameter making the assumption that particles are hard spheres, in the multiple diffusion regime, calculated with Mie theory, for different particle volume fractions (0.1%, 1% and 10%). In this figure, the scattering curve at $\phi = 1\%$ corresponds the one obtained at the end of the process and at the end of reagent addition for precipitations performed in double-jet stirred tank and using micromixer, respectively.

We observe an increase, a plateau and a decrease of backscattering values, and that, especially for high volume fraction.

For a given backscattering level, there are at least 2 solutions. For example, considering $\phi = 1\%$ curve, and for $BS = 30\%$ (close to backscattering level observed during boehmite precipitation), there are 3 solutions: $l = 0.06$ µm, $l = 0.08$ µm, $l = 12.41$ µm. However, only one solution is physically right.

In order to find this solution, another technique based on laser diffraction measurements was applied to suspension (Mastersizer 2000, MALVERN INSTRUMENTS). For boehmite suspension obtained in the double-jet stirred tank (reagents addition time: 30 min) the results are shown in Fig. 3. The Sauter diameter obtained was 11.37 µm and is in good agreement with the calculated Sauter diameter from the experimental backscattering level (12.41 µm). Thus, the right part of the curves of Fig. 2 has to be considered in this study.

Mie theory allows the calculation of an equivalent mean size which is in agglomerate scale. Indeed, the model is an interpretation of measured signals and considers monodispersed hard spheres with no interaction between them. These hypotheses are rather strong compared to the actual studied system. For this reason, in the following sections, the raw backscattered signals are given. These signals are a signature of all scattering objects in suspension, regardless of their size. Thus, measuring transmitted and backscattered levels during precipitation allows the evolution of the overall objects to be followed, considering all size scales.

2.4. Powder characterization techniques

2.4.1. Powder X-ray diffraction

The crystal phase identification was achieved by powder X-ray diffraction. Data were collected on a PANalytical X'Pert Pro θ–θ diffractometer in Bragg–Brentano geometry, using filtered *Cu K*α radiation ($\Lambda = 1.5418$ Å) and a graphite secondary-beam monochromator. Diffraction intensities were measured at room temperature by scanning from 2° to 72° with a step size of 0.05° (2θ). Crystallite sizes were determined by Scherrer's equation:

$$\varepsilon_{hkl} = \frac{K\lambda}{\cos\theta\sqrt{\Delta_r^2 - \Delta_0^2}} \tag{2}$$

where ε_{hkl} is the length of the crystallite along the direction defined by, (hkl), K the Scherrer constant ($K = 0.9$) [40]. This value is an approximation which suits with orthorhombic systems. Δ_r is a diffraction peak width of the sample, and Δ_0 is the width of the same peak due to the instrument, determined with LaB_6. The repeatability error was estimated to be 0.5 nm. The most representative particle morphology of boehmite has been determined using Debye formula [41]. Scherrer's formula cannot completely determine complex morphologies such as boehmite crystallites

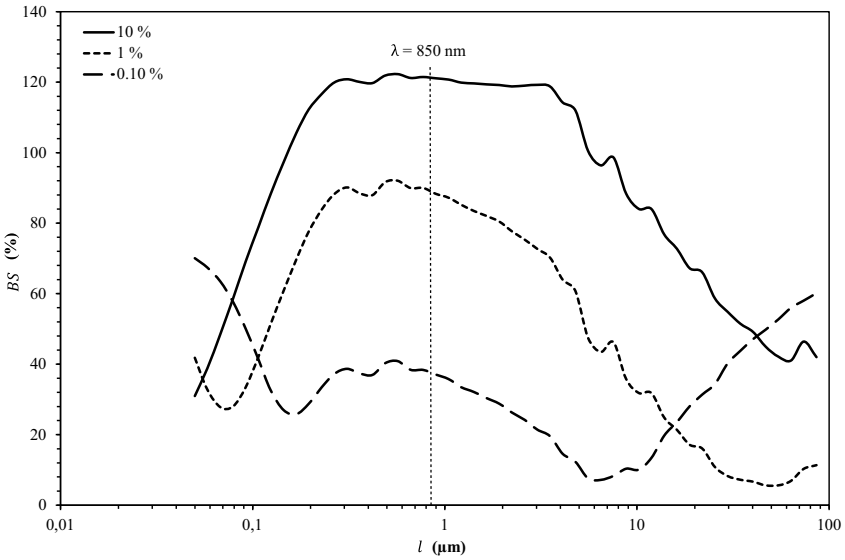

Fig. 2. Theoretical backscattering level *BS* versus particle surface mean diameter for particle volume fractions $\phi = 0.1\%$, $\phi = 1\%$, $\phi = 10\%$ ($\Lambda = 850$ nm, refractive index if dispersant $n_0 = 1.33$, refractive index of boehmite $n_p = 1.655$).

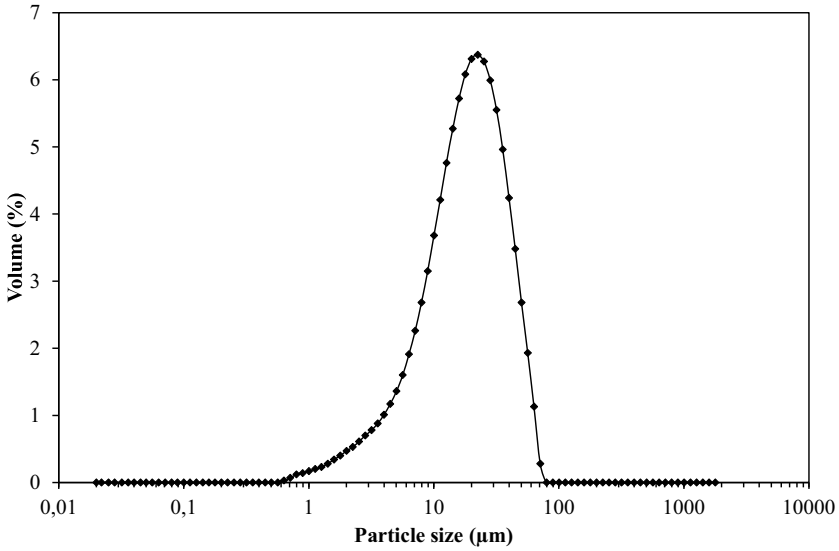

Fig. 3. Particle size distribution obtained with laser diffraction measurements for boehmite suspension synthesized with double-jet stirred tank device (reagents addition time: 30 min).

(hexagonal, diamond, truncated cube crystallite). Scherrer's equation was only used to calculate [020] and [120] directions, and thereby evaluate the thickness and a diagonal of boehmite crystallite.

2.4.2. N_2 adsorption–desorption

Nitrogen adsorption–desorption determine specific surface area, pore volume and porous diameter, which means space between primary crystallites/aggregates, in a range of micropores (<2 nm) to macropores (>50 nm). Differences in terms of isotherms, specific surface area, porous volume and porous diameter reveal differences in particle aggregation.

The nitrogen adsorption–desorption isotherms were collected at 77 K using an adsorption analyzer Micromeritics ASAP 2420. Analyzed samples were γ-alumina obtained after calcination of boehmite samples. Samples were previously dried under vacuum for 6 h at 110 °C. From the N_2 isotherm, the specific surface area (S_{BET}) was determined by the BET method in $0.10 \leqslant P/P_0 \leqslant 0.35$ domain, and pore size distributions were calculated with the BJH method (Barrett–Joyner–Halenda). The mean pore diameter d_{pBET} corresponds to the maximum pore size distribution (adsorption branch). Pore volume V_p was calculated from the adsorbed volume of gas V_{ads} at the higher relative pressure ($P/P_0 \to 1$) by:

$$V_p = \frac{\rho_{N_{2(g)}}}{\rho_{N_{2(l)}}} V_{ads} = 0.00155 \times V_{ads} \quad (3)$$

The errors associated with adsorption–desorption analyses were estimated to be 5% for the specific surface area (S_{BET}), 0.02 cm^3/g for pore volume V_p and 0.5 nm for pore diameter d_{pBET}.

2.4.3. Mercury porosimetry

Mesoporous volume V_{pHg} and mean pore diameter d_{pHg} were determined by mercury porosimetry, in the range of 3.75–7500 nm. The measures were acquired with a Micromeritics Autopore IV 9500.

The mean pore radius r^p was obtained with the following equation [42], with γ the surface tension of mercury and θ the angle of contact:

$$r^p = -\frac{2\gamma \cos\theta}{\Delta p} \quad (4)$$

2.4.4. Transmission electron microscopy

Transmission electron microscopy (TEM) observation were performed on a JEOL JEM1400 (120 kV) apparatus.

A small amount of boehmite powder was dispersed in ethanol. Then, a droplet was deposited on a carbon-coated grid and allowed to dry under a halogen lamp.

2.5. Supersaturation calculation

Supersaturation is the driving force for precipitation. It defines the state of a binary solute/solvent mixture when the solute concentration exceeds equilibrium.

For boehmite precipitation, following the reaction:

$$Al(OH)_4^- + \frac{1}{3}Al^{3+} \to \frac{4}{3}AlOOH + \frac{4}{3}H_2O \quad (5)$$

which can also be written as:

$$Al^{3+} + 2H_2O \to AlOOH + 3H^+ \quad (6)$$

Supersaturation S can be calculated with the equation:

$$S = \left(\frac{(a_+)^{\nu+} \cdot (a_-)^{\nu-}}{K_s}\right) = \left(\frac{(a_{Al^{3+}}) \cdot (a_{H^+})^3}{K_s}\right) \quad (7)$$

where a_+ and a_- are respectively the activity of cations and anions. ν^+ and ν^- re respectively the number of cations and anions in the equation of reaction. K_s is the solubility product.

The Pitzer equations [43], implemented in PHREEQC [45], were used to determine activity coefficients. In this model, the influence of specific ion interactions on the Gibbs free energy of the solution is expressed through a virial expansion of the activity coefficients:

$$\ln \gamma_i = \ln \gamma_i^{DH} + \sum_j \beta_{ij}(I) m_j + \sum_j \sum_k C_{ijk} m_j m_k + \ldots \quad (8)$$

where m is the molality, γ_i^{DH} is a modified Debye–Hückel activity coefficient. $\beta_{ij}(I)$ is like and unlike ion interactions coefficient that depends on the ionic strength I. C_{ijk} is the third virial coefficient taken independent of the ionic strength. A detailed description of the exact form of Eq. (8) is given in [44].

All interaction coefficients of the model used in this study were taken from the literature [46–49].

3. Results and discussion

3.1. Double-jet stirred tank precipitation

Backscattering relative intensity (*BS*) and transmission relative intensity (*TR*) were recorded during precipitation experiments. Representative curves of the measured backscattering and transmission levels are given in Fig. 4. With this device, reagent addition took 30 min. Before addition, *BS* and *TR* levels were those in water (*BS* ≈ 69% and *TR* ≈ 73%), considering glass cell reflections. When starting the addition, both levels dropped. The transmission intensity decreased until it reached 0%: particles appeared in the system and reached a concentration such that light cannot be transmitted anymore. The backscattering intensity (*BS*) decreased with the apparition of particles, and then increased while particles were still appearing in the environment. The first part of the *BS* curve, shown as a dotted line in Fig. 4, cannot be considered as a correct *BS* value since the transmission phenomenon was still occurring. When *TR* reaches zero, light does not cross the tube and reflections of the glass tube become negligible. *BS* can be considered for further calculations (full line).

The backscattering intensity depends on both particles volume fraction ϕ and particle diameter *l*. Since reagents are added throughout the precipitation, ϕ is not constant, and increases linearly because of constant reagent flows; *BS* variations can be explained by an increase of the particle volume fraction but also by a change in the characteristic length *l* of the aggregate in the medium. At the end of the experiment, the particle volume fraction ϕ = 1% and *BS* = 32.4%.

A TEM micrograph of dried boehmite obtained by double-jet stirred tank precipitation is shown in Fig. 5. Boehmite particles present a fibrous morphology, which is correlated with previous works: when using aluminum sulfate $Al_2(SO_4)_3$ as reagent, sulfate ions would bind to boehmite by hydrogen bonds [11] because of their high affinity with aluminum. A probable mechanism of aggregation of boehmite crystallites in the presence of sulfate ions is presented in Fig. 6. The formation of fibers is the result of a first directed aggregation of crystallites due to the presence of sulfate ions. Then these fibers stick together to form a disordered fiber-bundle network. The analyzed material is dried, thus the micrograph does not represent the aggregate state of fibers in the suspension. However, fiber length should be the same in suspension. Fibers have a length between 30 and 60 nm.

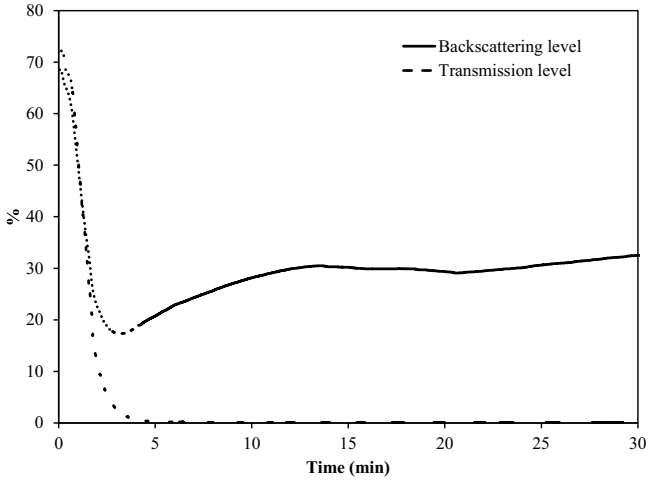

Fig. 4. Temporal evolution of the backscattering and transmission levels during boehmite precipitation performed in double-jet stirred tank device.

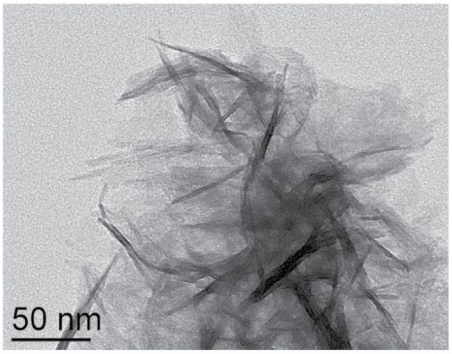

Fig. 5. Transmission electron microscopy micrograph of dried boehmite prepared in double-jet stirred tank device (reagents feeding time of 30 min).

3.2. Micro-mixer precipitation

For following aggregation of boehmite during the precipitation process performed using micro-mixer, the suspension was withdrawn from the vessel and analyzed with the Turbiscan On Line, once the particles had precipitated in the micro-mixer and fell in the stirred tank (total time of 30 min). The time of reagent addition t_{ea} was 1 min 32 s. Because of the higher supersaturation level in the mixer, particles appear in the vessel faster than with the previous experimental setup. Consequently, the transmission level reaches a null level instantaneously while the backscattering level decreases suddenly and increases until the end of addition (see Fig. 7). The increase of the back scattering level is mainly due to the increase of the volume fraction of solids. At the end of the reagent addition, when $>t_{ea}$, ϕ is constant in the vessel (ϕ = 1%). *BS* variations are thus only due to the variation of the characteristic size of the aggregates. The decrease of the backscattering level, when $>t_{ea}$, can be attributed to a change in the structure of the aggregates in the medium.

At the end of the process, the backscattering level reaches a constant value corresponding to *BS* = 23.9%. This value is lower than the one obtained for the suspension precipitated in the double-jet stirred tank (*BS* = 32.4%), which supports that different types of aggregates are formed in suspension during these two types of precipitation.

In the following sections, only *BS* level will be considered for precipitations performed with micro-mixer devices since the *T* level immediately reached zero in all cases. Thus, *BS* variation has a physical meaning related to aggregate structuration.

3.3. Comparison of the two types of precipitation

Boehmite powders (XRD) and γ-alumina (N_2 adsorption–desorption) obtained at the end of synthesis with the two types of precipitation are characterized to compare the product properties (Table 3).

For the two samples, the only detected phase on XRD patterns (Fig. 8) was boehmite. Peaks have similar width and taking all the caution linked to the errors of estimation, similar crystallite dimensions are obtained, as presented in Table 3.

The specific surface area (S_{BET}) was about 290 ± 15 m^2/g for double-jet stirred tank alumina and lower for precipitation performed with micromixer (228 ± 11 m^2/g). Differences were observed for V_p and, d_{pBET} which were significantly lower for micromixer obtained alumina (V_p = 0.37 cm^3/g, d_{pBET} = 6.4 nm) than for double-jet stirred tank alumina (V_p = 1.06 cm^3/g, d_{pBET} = 12 nm). N_2 adsorption/desorption isotherms (Fig. 9) show porosity differences. The double-jet stirred tank product isotherm

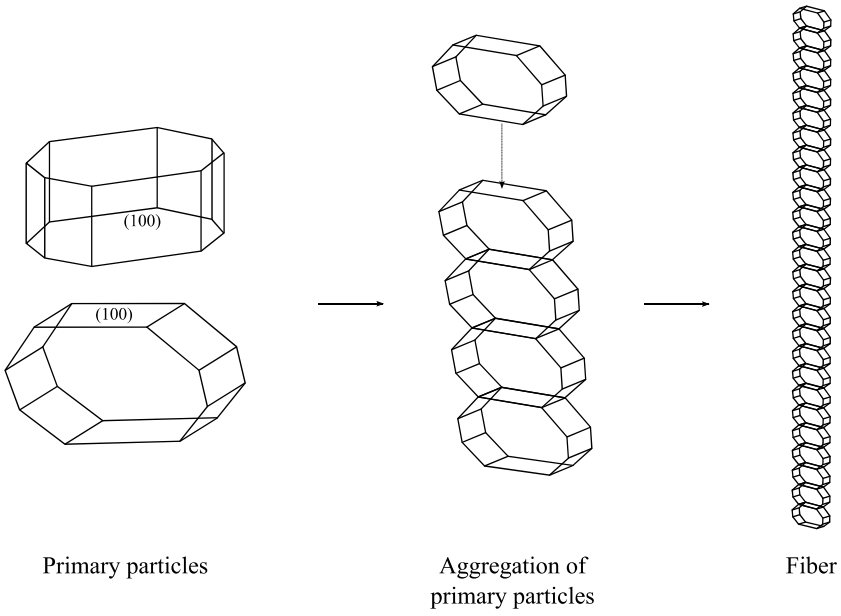

Fig. 6. Representation of the probable aggregation of boehmite nanoparticles in presence of sulfate ions.

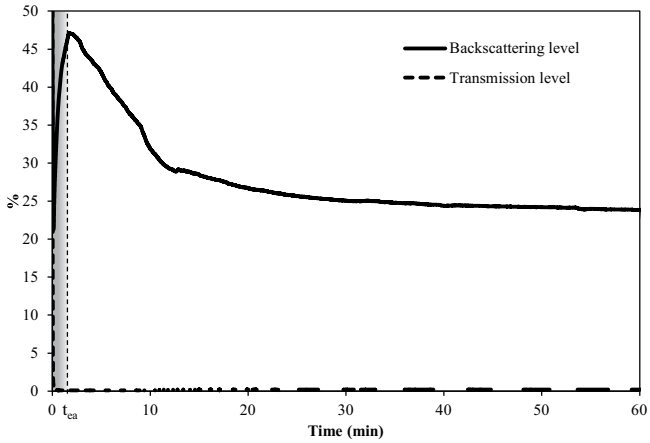

Fig. 7. Temporal evolution of backscattering and transmission measured levels during precipitation performed in Hartridge–Roughton micro-mixer.

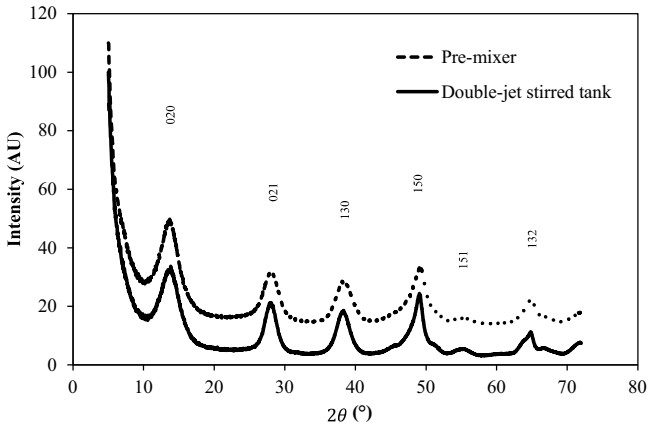

Fig. 8. Diagrams obtained by XRD technique of boehmite synthesized with double-jet stirred tank and Hartridge–Roughton micro-mixer.

was of type II with a H_3 hysteresis loop, which is characteristic of slit-shaped pores, and micromixer precipitate isotherm is of type IV with a H_2 hysteresis loop. This type of loop is observed for tubular or bottle-shaped pores. BJH pore size distribution (PSD) was larger for the double-jet stirred tank product than for the micromixer alumina which presents narrower PSD and lower pore sizes (Fig. 9B).

Initial supersaturation was calculated for both precipitation routes, with PHREEQC, using the Pitzer model. For the double-jet stirred tank, in order to be able to calculate initial supersaturation considering water in the vessel, a quantity of introduced reagents perfectly mixed corresponding arbitrarily to an increment of feeding time (5 s) is taken. In that case, the initial supersaturation S_i was 288. For the micro-mixer, initial supersaturation was constant during the feeding since the environment in which the reagents meet was the same: S_i = 19,953. The difference in the initial supersaturation means that particles are formed in a different environment. Considering a double-jet stirred tank, particles were formed in a less concentrated medium in ions than in the micro-mixer. This can have an effect of interaction between particles, and thus on their aggregation.

This reasoning was confirmed by porosity differences between boehmites obtained from the two devices, which are explained by a different aggregates structure, considering the same

Table 3
Initial supersaturation during precipitation and characteristics of synthesized boehmites (boehmite crystallite dimension and corresponding alumina textural properties) for precipitation performed in double-jet stirred tank and Hartridge–Roughton micromixer.

	S_i	ε_{020} (nm)	ε_{120} (nm)	S_{BET} (m^2/g)	V_p (cm^3/g)	V_{pHg} (cm^3/g)	d_{pBET} (nm)	d_{pHg} (nm)
Double-jet stirred tank	288	2.2	2.9	291	1.06	0.63	12	11
Hartridge–Roughton micromixer	19,953	2.8	2.9	228	0.37	0.31	6.4	6.8

ε_{020} and ε_{120} (±0.5 nm): boehmite crystallite size in the direction respectively (020) and (120) estimated by the Scherrer's formula.

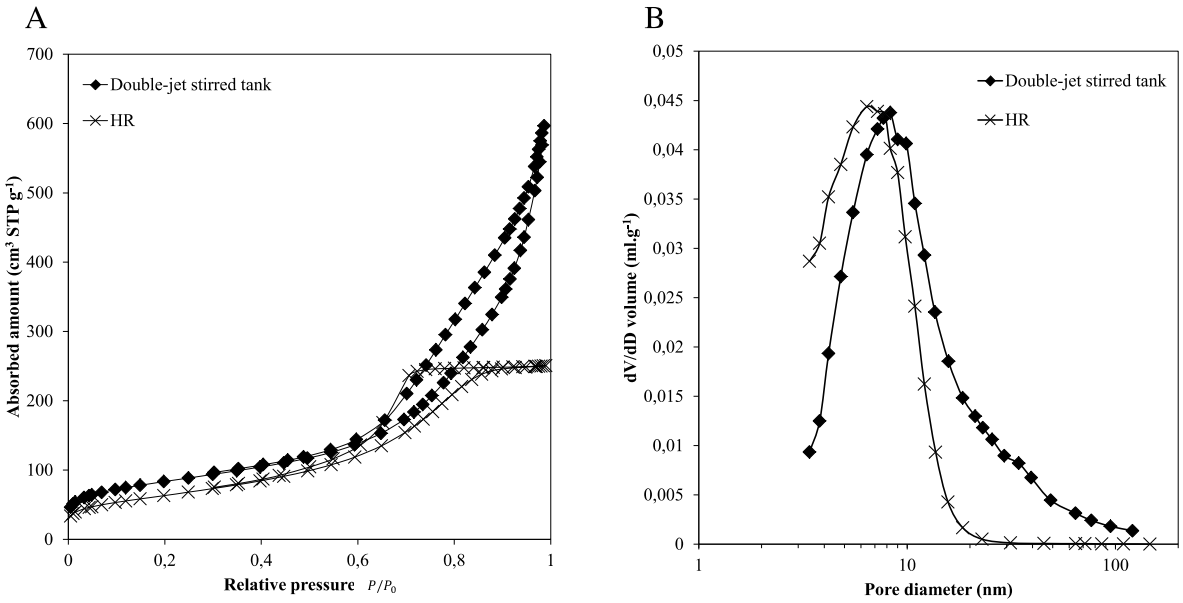

Fig. 9. Nitrogen adsorption–desorption isotherms (A), recorded at 77 K, and BJH pore size distribution (adsorption branch) (B) for alumina obtained in double-jet stirred tank and Hartridge–Roughton devices.

crystallites sizes. This could be due to fiber aggregation or to different fiber lengths (aggregation of primary particles). Thus, the micro-mixing step has a huge influence on material porosity since it affects aggregation via higher initial supersaturation.

3.4. Precipitation in micro-mixer: effect of mixing parameters

Effect of feeding flowrate in the micro-mixer, vessel stirring rate after reagents addition and micro-mixer type are studied at isosupersaturation in the vessel (S_i = 19,953).

3.4.1. Influence of feeding flow

Changing feeding flowrate changes the mixing intensity, which is described by the Reynolds number and the residence time in micro-mixer. Hartridge–Roughton micromixer was tested with three Reynolds numbers (*Re*): 8×10^3, 15×10^3 and 20×10^3. The corresponding mixing and alumina porosity characteristics are presented in Table 4.

Backscattering levels are presented in Fig. 10 from the time t_{ea}, ϕ is constant. For every *Re*, *BS* decreases until reaching a constant level. The higher *Re*, the more important the decrease in the slope is and the faster the constant level is reached; that is to say, aggregates are formed quickly for higher *Re*. Constant levels are slightly lower with high *Re* (25.1% for F1, 20.0% for F2, 19.7% for F3).

These close results are reflected in corresponding alumina porosity. S_{BET} is slightly higher with high *Re* (228 m^2/g for F1, 255 m^2/g for F3), but V_{pHg} and d_{pHg} are similar for each *Re*, considering instrument errors.

In previous works of the literature, the effect of feeding rate was studied for a Hartridge–Roughton micro-mixer (1 mm inlet tubes,

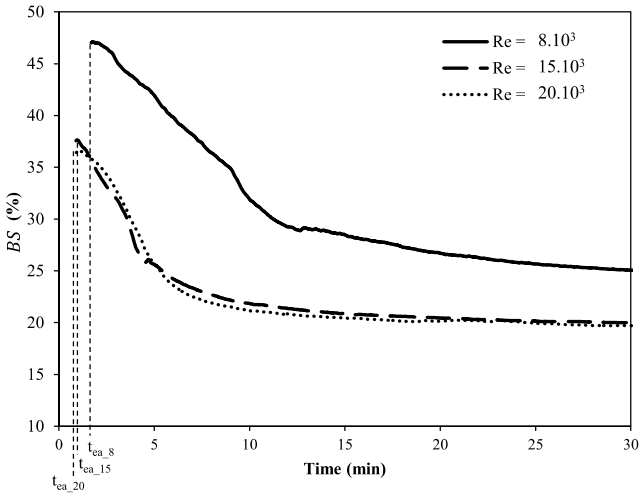

Fig. 10. Temporal evolution of backscattering levels during precipitation performed in Hartridge–Roughton for three Reynolds number (*Re* = 8×10^3, *Re* = 15×10^3, *Re* = 20×10^3.)

2 mm outlet tube), with a rate similar to the one used in this study [50]. The authors found that average agglomerate size was smaller (laser diffraction measurement) for a feed rate of 1000 ml/min, compared to lower feed rates. In the lower range of feed rates, random variation was observed. Globally, agglomerate sizes are close.

Mixing level in a micro-mixer does not seem to have a huge effect on *BS* constant levels and therefore on aggregate size *l* and material porosity. This is probably due to the fact that mixing is so efficient, even for low feed rates, that it does not affect any

Table 4
Mixing and boehmite/alumina characteristics for syntheses with three reagents feed rates in Hartridge–Roughton micro-mixer.

	Feed rate (ml/min)	HR Reynolds number	Reagents addition time t_{ea} (s)	HR residence time (ms)	S_{BET}* (m^2/g)	V_{pHg}* (cm^3/g)	d_{pHg}* (nm)
F1	437	8×10^3	92	26	228 ± 11	0.31	6.7
F2	804	15×10^3	50	14	244 ± 12	0.32	6.4
F3	1058	20×10^3	38	10	255 ± 13	0.31	6.1

* Porosity characteristics for γ-alumina.

precipitation stages (nucleation/growth, aggregation) and therefore material properties.

3.4.2. Influence of the stirring rate in the vessel after micro-mixing step

Influence of vessel stirring during "standard" precipitation has been extensively studied in the literature [33,50,51], but its effect on the ripening phase after the reagents addition, especially when a micro-mixer device is used, has been much less well investigated.

Three different stirring rates were studied here, corresponding to the characteristic vessel Reynolds numbers: $Re_v = 19 \times 10^3$, 52×10^3 and 76×10^3. Mixing characteristics and corresponding boehmite/alumina properties are presented in Table 5. For each stirring rate, Kolmogorov scales L_K were calculated with the following equation, with v the kinematic viscosity of the continuous phase (water at 50 °C: $v = 55.6 \times 10^7$ m^2 s^{-1}) and ϵ the dissipated power per mass unit:

$$L_K = \left(\frac{v^3}{\epsilon}\right)^{1/4} \quad (9)$$

Backscattering levels are shown in Fig. 11, after time t_{ea}.

For each experiment, *BS* decreased and reached a constant level. For S1 and S2 experiments, the corresponding curves were very similar. For the highest stirring rate (S3), the decreasing slope was steeper and the curve reached a constant level slightly earlier than for S1 and S2. For each experiment, constant levels were really close (26.0% for S1, 25.1% for S2, 25.0% for S3).

Specific surface area was higher for the lowest stirring rate ($S_{BET} = 268 \pm 13$ m^2/g for S1), but V_{pHg} and l were the same for the different materials, which is in correlation with the close *BS* values.

The stirring rate parameter followed by Turbiscan On Line does not seem to have an effect on precipitation. This result is not intuitive, however, because we could expect that high stirring rate could break aggregates and results in higher *BS*. In a micro-mixer, crystallites precipitate and then form aggregates and maybe agglomerates.

A first hypothesis could be that agglomerates, constituted of aggregates (fibers), are dispersed when they fall in the stirred vessel, until only isolated aggregates or indivisible aggregates of fibers are in suspension, which would explain the constant level. However, considering this hypothesis, agglomerate breakage would be significantly faster with high stirring speed (S3) since they are not structured with strong interactions, but this was not observed. Moreover, if breakage was responsible for object size decreases, the aggregates obtained would have a size close to Kolmogorov scales L_K. This is not the case though, because sizes obtained by Turbiscan On Line are in the ten micrometer scale, and calculated L_K are at least double. The objects in suspension were smaller than Kolmogorov scale.

The other hypothesis is that aggregates (fibers) fall in vessel and structure of aggregates varies until reaching a certain dimension (constant level) (due to the number of fibers in the ball or the entanglement of fibers). This structuration would not be influenced by stirring rate because it concerns strong interactions. Thus, a decrease in the phase of *BS* would be due to time, as a short ripening phase.

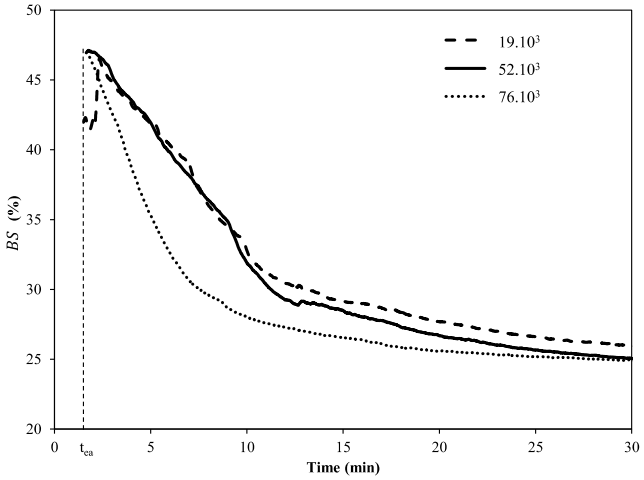

Fig. 11. Temporal evolution of backscattering levels during precipitation performed in Hartridge–Roughton micro-mixer for three Reynolds number ($Re_v = 19 \times 10^3$, $Re_v = 52 \times 10^3$, $Re_v = 76 \times 10^3$.)

3.4.3. Influence of micro-mixer type

Two types of micromixers were tested: Hartridge–Roughton (HR) and Y shape. HR and Y micro-mixing times t_μ have been determined in the literature: t_μ (HR) = 1.2 ms and t_μ (Y) = 3.8 ms (1 mm inlet tubes, 2 mm outlet, 90° angle for Y, fluid velocity of 15 m s^{-1} in the central tube) [37]. Y mixer presents worse micro-mixing than HR. In this part, the precipitation in Y mixer was studied for the same operating conditions than for HR precipitation (Section 3.2).

Backscattering levels for both micro-mixers were shown in Fig. 12(A). Obviously, *BS* curves were similar for HR and Y precipitations in the same conditions. At the end of precipitation (30 min), the values of *BS* were close: 23.6% for Y and 25.1% for HR.

The specific surface area was slightly higher for Y1 ($S_{BET} = 245 \pm 12$ m^2/g) than for HR ($S_{BET} = 228 \pm 11$ m^2/g), but V_{pHg} and d_{pHg} are very close.

Even if Y produces less efficient mixing than HR, the mixing seems to be efficient enough to not have an effect on aggregation and therefore on material porosity.

Feed rate influence using Y mixer was studied for two values of *Re* number (Table 6). The end addition times t_{ea} for each case are represented in Fig. 12B. The backscattering intensity curves (Fig. 12B) have the same evolutions, and reach similar value at the end of the experiments (*BS* = 23.5%).

Porosity was the same for both materials. These elements justify the hypothesis that the mixing is efficient enough in the case of micro-mixers to not affect aggregation and thus material properties. Lower flow rates, at the same reagent concentrations, could not be studied because of micro-mixer clogging.

Table 5
Mixing and boehmite/alumina characteristics for synthesis with three vessel stirring rate performed in Hartridge–Roughton micro-mixer.

	Stirring rate (rpm)	Vessel Reynolds number Re_v	Vessel stirring power (W/m^3)	L_K (μm)	S_{BET}* (m^2/g)	V_{pHg}* (cm^3/g)	d_{pHg}* (nm)
S1	100	19×10^3	12	69	268 ± 13	0.33	6.3
S2	270	52×10^3	250	29	228 ± 11	0.31	6.7
S3	400	76×10^3	800	22	244 ± 12	0.35	6.3

* Porosity characteristics for γ-alumina.

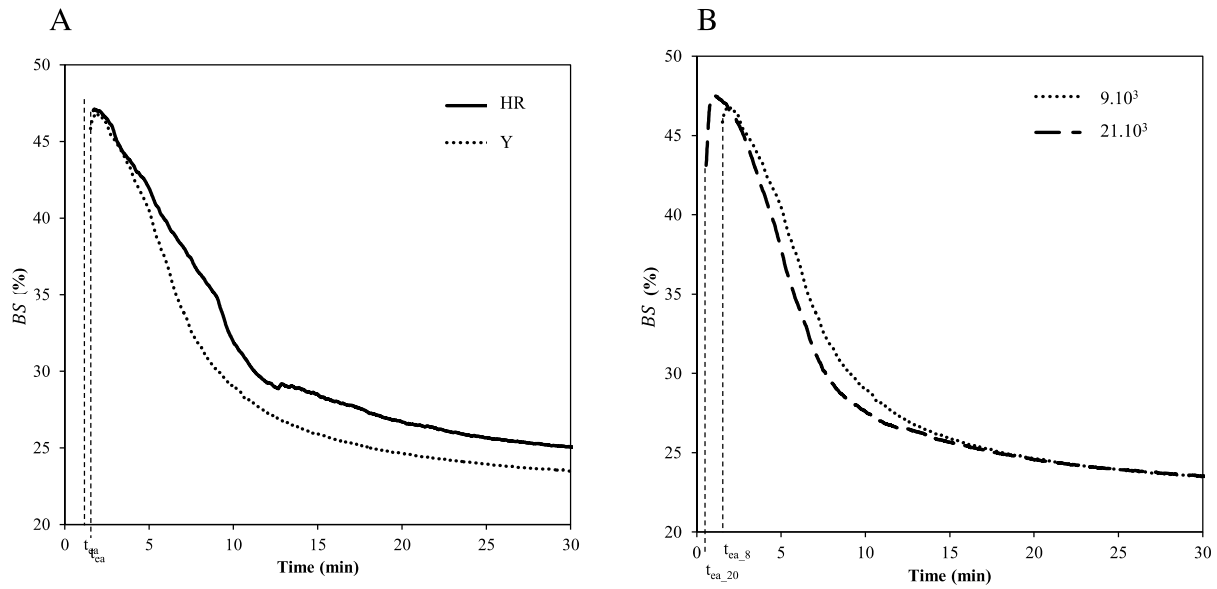

Fig. 12. Temporal evolution of the backscattering relative intensity for precipitation experiments performed in Hartridge–Roughton and Y micro-mixers geometries (A) and for two Reynolds number in Y micro-mixer ($Re = 9 \times 10^3$, $Re = 21 \times 10^3$) (B).

Table 6
Mixing and boehmite/alumina characteristics for precipitation performed in Y micro-mixer, for two reagents feed rate.

	Feed rate (ml/min)	Micro-mixer Reynolds number	Reagents addition time (s)	Y residence time (ms)	S_{BET}* (m^2/g)	V_{pHg}* (cm^3/g)	d_{pHg}* (nm)
Y1	503	9×10^3	93	23	245 ± 12	0.32	6.4
Y2	1116	21×10^3	50	10	242 ± 12	0.30	6.4

* Porosity characteristics for γ-alumina.

Table 7
Characteristics of synthesized boehmites/aluminas and initial supersaturation.

Reagents addition time (min)	S_i	ε_{020} (nm)	ε_{120} (nm)	S_{BET}* (m^2/g)	V_{pHg}* (cm^3/g)	d_{pHg}* (nm)
6	1175	1.9	2.4	280 ± 14	0.27	5.5
10	741	2.0	2.5	295 ± 15	0.34	5.7
20	407	2.2	2.6	280 ± 14	0.47	9.5
30	288	2.2	2.9	291 ± 15	0.63	11.1
240	51	2.7	4.1	292 ± 15	0.73	7.8

ε_{020} and ε_{120} (±0.5 nm): boehmite crystallite size in the direction respectively (020) and (120) estimated by the Scherrer's formula.
* Porosity characteristics for γ-alumina.

3.5. Effect of feed time in double-jet stirred-tank precipitation

Main differences between double-jet stirred tank precipitation and using micro-mixing device are the pre-mixing stage on the one hand, and the reagent feed time on the other hand. This last parameter has been studied here for reagent feed times from 6 to 240 min, for double-jet stirred tank precipitation.

In this device, feed time has an effect on supersaturation. The local supersaturation near the zones where reagents arrive in the vessel is not the same for different addition times. For a long addition time, droplets added in the vessel are more dispersed in the vessel before the following droplets fall. Therefore, local supersaturation is lower in the feeding points than in the case of short addition time. Initial supersaturation S_i after 5 s of addition was calculated for different addition times, considering a perfectly mixed system (pH = 9 at the end of simulation). The results are presented in Table 7. Supersaturation decreased with an increased feeding time. Considering constant vessel stirring, the faster the addition, the slower the reagents are locally dispersed in water and the higher supersaturation is. It is important to note that, in reality, mixing is not homogeneous and supersaturation is different in the vessel [33]. A perfectly mixed system is considered for thermodynamic calculations, whereas in reality, supersaturation is locally higher than calculated. In that case, initial supersaturation for 6 min was higher than calculated and became closer to micro-mixer supersaturation (S_i = 19,953).

Backscattering levels throughout precipitation are presented in Fig. 13. Curves are plotted from the time when the transmission level was equal to zero. The volume fraction ϕ was not the same at time t between experiments and increased during precipitation. For additional time from 6 to 30 min, *BS* increased. The slope is higher for smaller addition times. For an addition time of 240 min, *BS* increased and then slowly decreased.

Boehmite crystallites sizes were obtained by XRD measurements for each experiment (Table 7). Considering uncertainty of Scherrer's equation results, we see a trend: both ε_{020} and ε_{120}

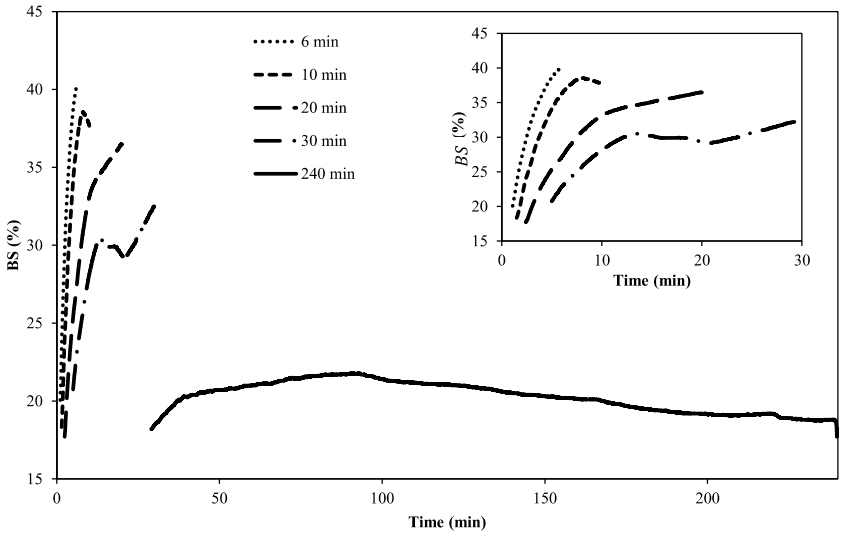

Fig. 13. Temporal evolution of the backscattering relative intensity for different reagents addition time in a double-jet stirred tank device.

would increase with addition time. Two factors can explain these results. The first could be ripening. In each case, all of the particles did not have the same residence time in the vessel. The first particles formed in the vessel undergo a ripening phase compared to the last particles precipitated, which can explain why particles are bigger following the longest addition times. Another factor is supersaturation. Initial supersaturation decreased with feeding time. However, in accordance with the classical theory of nucleation, higher supersaturation leads to higher number of formed crystallites, to the detriment of growth.

Specific surface areas are equivalent for all experiments, considering instrument errors. However, mesoporous volume V_{pHg} significantly increased when increasing addition time. Mean pore diameter d_{pHg} increased and doubled for addition times from 6 to 30 min. For an addition time of 240 min, d_{pHg} is slightly lower (d_{pHg} = 7.8 nm).

Similar crystallite sizes are correlated with similar specific surface areas. The differences met for V_{pHg} and d_{pHg} are thus explained by a different structuration of crystallites. For shorter addition times, mesoporous volume was lower, showing a more compact material. For an addition time of 240 min, d_{pHg} did not follow the same trend and was lower. This could be due to the ripening effect, which is more important than in the other experiments. Aggregates are smaller because they are more compact, explaining the smaller mean pore diameter. Considering equivalent specific surface areas between experiments, the pore number was much higher for an addition time of 240 min since d_{pHg} was smaller but V_{pHg} was higher.

It is interesting to note that for a lower feeding time (6 min), V_{pHg} and d_{pHg} were closer to those of micro-mixers. This operating condition corresponds to the highest initial supersaturation for double-jet stirred tank experiments. Even though the true experimental initial supersaturation for 6 min was not the one calculated because of the not perfectly mixed medium, and is supposed to be higher than calculated, it was still lower than micro-mixer supersaturation. Moreover, we have seen in previous experiments that mixing has no effect on aggregation for micro-mixer experiments, possibly because of a sufficiently high supersaturation. The similar porosity in terms of porous volume and mean pore diameter for these both experiments confirmed that S_i = 1175 is a threshold beyond which aggregation is the same, regardless of the operating conditions.

Feed time, via supersaturation, has an effect on material porosity. In the range of 6–30 min feeding, mesoporous volume and mean pore diameter increased with addition time, due to the different aggregation of crystallites. For an addition time of 240 min, the trend was different and the mean pore diameter was lower than expected, probably due to the ripening phase.

4. Conclusion

Precipitation of boehmite was studied in two devices, double-jet stirred tank and micro-mixing (HR and Y), and the influence on operating conditions on the product quality was analyzed. Precipitation kinetics were followed by multiple light scattering, by considering backscattering levels.

The main differences of precipitation conditions performed in the two devices are mixing and supersaturation level. Boehmite obtained by micro-mixing, at high supersaturation, presents lower specific surface area, mesoporous volume and mean pore diameter than materials produces using the double-jet stirred tank, while the crystallite size was similar for both boehmites. Aggregation dynamics or mechanisms are then different, maybe at different scales (primary crystallite, fibers), which could be directly due to supersaturation.

Mixing in micro-mixer at isosupersaturation (feeding flow in micro-mixer, stirring power, micro-mixer type) has no effect on boehmite quality in the studied range.

Reagents feed effect was studied for double-jet stirred tank precipitation, where supersaturation levels are much lower than using a micromixer. Supersaturation, via feeding rate, had an effect on boehmite properties by increasing porosity at low supersaturation.

The similarities in quality between boehmite obtained at the highest supersaturation in double-jet stirred tank and the one obtained with micromixer would suggest that there is a supersaturation threshold value beyond which aggregation is blocked and process operating parameters do not affect porosity anymore.

Turbiscan On Line allowed characterizing the differences between objects in suspension during precipitation operation, and constitutes a powerful sensor to follow precipitation process. It presents the advantage of giving a signature of the aggregation state of the particles before the filtration–washing–drying steps which can change this aggregation.

References

[1] B.C. Lippens, J.H. De Boer, Study of phase transformations during calcination of aluminum hydroxides by selected area electron diffraction, Acta Crystallogr. 17 (1964) 1312–1321, http://dx.doi.org/10.1107/S0365110X64003267.

[2] R. Tipakontitikul, A. Niyompan, K. Srisurat, N. Kanchanarat, T. Tunkasiri, Effect of pH en phase formation and morphology of the nanocrystalline boehmite powder prepared by a precipitation method, J. Microsc. Soc. Thail. 22 (2008) 20.

[3] P. Alphonse, M. Courty, Structure and thermal behavior of nanocrystalline boehmite, Thermochim. Acta 425 (2005) 75–89, http://dx.doi.org/10.1016/j.tca.2004.06.009.

[4] X. Bokhimi, A. Morales, J.S. Valente, Sulfate ions and boehmite crystallization in a sol made with aluminum tri-sec-butoxide and 2-propanol, J. Phys. Chem. C 111 (2007) 103–107, http://dx.doi.org/10.1021/jp0611673.

[5] S. Musić, D. Dragčević, S. Popović, N. Vdović, Microstructural properties of boehmite formed under hydrothermal conditions, Mater. Sci. Eng. B 52 (1998) 145–153, http://dx.doi.org/10.1016/S0921-5107(97)00277-8.

[6] Y. Mathieu, B. Lebeau, V. Valtchev, Control of the morphology and particle size of boehmite nanoparticles synthesized under hydrothermal conditions, Langmuir 23 (2007) 9435–9442, http://dx.doi.org/10.1021/la700233q.

[7] L. Zhang, X. Jiao, D. Chen, M. Jiao, γ-AlOOH nanomaterials with regular shapes: hydrothermal fabrication and Cr_2O_{72} – adsorption, Eur. J. Inorg. Chem. 2011 (2011) 5258–5264, http://dx.doi.org/10.1002/ejic.201100793.

[8] K.P. Prodromou, A.S. Pavlatou-Ve, Formation of aluminum hydroxides as influenced by aluminum salts and bases, Clays Clay Miner. 43 (1995) 111–115.

[9] K. Hellgardt, D. Chadwick, Effect of pH of precipitation on the preparation of high surface area aluminas from nitrate solutions, Ind. Eng. Chem. Res. 37 (1998) 405–411, http://dx.doi.org/10.1021/ie970591a.

[10] J.-F. Hochepied, P. Nortier, Influence of precipitation conditions (pH and temperature) on the morphology and porosity of boehmite particles, Powder Technol. 128 (2002) 268–275, http://dx.doi.org/10.1016/S0032-5910(02)00178-X.

[11] Y. Xia, L. Zhang, X. Jiao, D. Chen, Synthesis of γ-AlOOH nanocrystals with different morphologies due to the effect of sulfate ions and the corresponding formation mechanism study, Phys. Chem. Chem. Phys. 15 (2013) 18290–18299, http://dx.doi.org/10.1039/C3CP53110D.

[12] D. Panias, A. Krestou, Effect of synthesis parameters on precipitation of nanocrystalline boehmite from aluminate solutions, Powder Technol. 175 (2007) 163–173, http://dx.doi.org/10.1016/j.powtec.2007.01.028.

[13] J.-M. Rousseaux, H. Muhr, E. Plasari, Chemical reactors of special geometry for the precipitation of mineral particles, Can. J. Chem. Eng. 78 (2000) 650–662, http://dx.doi.org/10.1002/cjce.5450780407.

[14] N. Bénet, H. Muhr, E. Plasari, J. Rousseaux, New technologies for the precipitation of solid particles with controlled properties, Powder Technol. 128 (2002) 93–98, http://dx.doi.org/10.1016/S0032-5910(02)00175-4.

[15] D. Ilievski, M. Rudman, G. Metcalfe, The separate roles of shear rate and mixing on gibbsite precipitation, Chem. Eng. Sci. 56 (2001) 2521–2530.

[16] G. Févotte, In situ Raman spectroscopy for in-line control of pharmaceutical crystallization and solids elaboration processes: a review, Chem. Eng. Res. Des. 85 (2007) 906–920, http://dx.doi.org/10.1205/cherd06229.

[17] H. Wikström, P.J. Marsac, L.S. Taylor, In-line monitoring of hydrate formation during wet granulation using Raman spectroscopy, J. Pharm. Sci. 94 (2005) 209–219, http://dx.doi.org/10.1002/jps.20241.

[18] A.A. Gowen, C.P. O'Donnell, P.J. Cullen, S.E.J. Bell, Recent applications of chemical imaging to pharmaceutical process monitoring and quality control, Eur. J. Pharm. Biopharm. 69 (2008) 10–22, http://dx.doi.org/10.1016/j.ejpb.2007.10.013.

[19] F. Lewiner, J.P. Klein, F. Puel, G. Févotte, On-line ATR FTIR measurement of supersaturation during solution crystallization processes. Calibration and applications on three solute/solvent systems, Chem. Eng. Sci. 56 (2001) 2069–2084, http://dx.doi.org/10.1016/S0009-2509(00)00508-X.

[20] M.L. MacCalman, K.J. Roberts, C. Kerr, B. Hendriksen, On-line processing of pharmaceutical materials using in situ X-ray diffraction, J. Appl. Crystallogr. 28 (1995) 620–622.

[21] H. Wu, M.A. Khan, Quality-by-design: an integrated process analytical technology approach to determine the nucleation and growth mechanisms during a dynamic pharmaceutical coprecipitation process, J. Pharm. Sci. 100 (2011) 1969–1986, http://dx.doi.org/10.1002/jps.22430.

[22] M. Li, D. Wilkinson, K. Patchigolla, P. Mougin, K.J. Roberts, R. Tweedie, On-line crystallization process parameter measurements using ultrasonic attenuation spectroscopy, Cryst. Growth Des. 4 (2004) 955–963, http://dx.doi.org/10.1021/cg030041h.

[23] H. Geers, W. Witt, Opus Ultrasonic Extinction: Fields of Application, Brighton, UK, 1998.

[24] M. Stintz, F. Hinze, S. Ripperger, Characterization of Concentrated Dispersions and Colloidal Systems by Acoustic Attenuation Spectroscopy and Colloid Vibration Potential, Brighton, UK, 1998.

[25] F. Alba, G.M. Crawley, D.M. Higgs, P.G. Kippax, Acoustic Attenuation Spectroscopy for Particle Sizing of High Concentration Dispersions, Brighton, UK, 1998.

[26] P. Snabre, L. Haider, M. Boynard, Ultrasound and light scattering from a suspension of reversible fractal clusters in shear flow, Eur. Phys. J. E 1 (2000) 41–53.

[27] P.J. Coghill, M.J. Millen, S. Rainey, B.D. Sowerby, On-line measurement of particle size in fine slurries, World Congress on Particle Technology 3, Brighton, UK, 1998.

[28] R.W. O'Brien, W.N. Rowlands, S.E. Gibb, T.A. Wade, R.J. Hutner, The electroacoustic method for determining particle size and charge, World Congress on Particle Technology 3, Brighton, UK, 1998.

[29] H. Buron, O. Mengual, G. Meunier, I. Cayré, P. Snabre, Optical characterization of concentrated dispersions: applications to laboratory analyses and on-line process monitoring and control, Polym. Int. 53 (2004) 1205–1209, http://dx.doi.org/10.1002/pi.1231.

[30] P. Snabre, A. Arhaliass, Anisotropic scattering of light in random media: incoherent backscattered spotlight, Appl. Opt. 37 (1998) 4017–4026.

[31] C. Bordes, F. Garcia, C. Frances, B. Biscans, P. Snabre, The on-line optical investigation of concentrated dispersions in precipitation and grinding processes, KONA Powder Part. J. 19 (2001) 94–108.

[32] C. Bordes, P. Snabre, C. Frances, B. Biscans, Optical investigation of shear- and time-dependent microstructural changes to stabilized and depletion-flocculated concentrated latex sphere suspensions, Powder Technol. 130 (2003) 331–337.

[33] J. Baldyga, J.R. Bourne, Interactions between mixing on various scales in stirred tank reactors, Chem. Eng. Sci. 47 (1992) 1839–1848, http://dx.doi.org/10.1016/0009-2509(92)80302-S.

[34] J. Bakldyga, W. Podgórska, R. Pohorecki, Mixing-precipitation model with application to double feed semibatch precipitation, Chem. Eng. Sci. 50 (1995) 1281–1300, http://dx.doi.org/10.1016/0009-2509(95)98841-2.

[35] R. David, B. Marcant, Prediction of micromixing effects in precipitation: case of double-jet precipitators, AIChE J. 40 (1994) 424–432, http://dx.doi.org/10.1002/aic.690400306.

[36] H. Hartridge, F.J.W. Roughton, A method of measuring the velocity of very rapid chemical reactions, Proc. R. Soc. Lond. Ser. A 104 (1923) 376–394, http://dx.doi.org/10.1098/rspa.1923.0116.

[37] M. Bertrand-Andrieu, E. Plasari, P. Baron, Methods for the characterization and comparison of mixing efficiency of different confined opposing jet mixing devices, in: 12th Eur. Conf. Mix., Bologna, Italy, 2006, p. 671.

[38] Y. Liu, C. Cheng, R.K. Prud'homme, R.O. Fox, Mixing in a multi-inlet vortex mixer (MIVM) for flash nano-precipitation, Chem. Eng. Sci. 63 (2008) 2829–2842.

[39] C. Lindenberg, J. Schöll, L. Vicum, M. Mazzotti, J. Brozio, Experimental characterization and multi-scale modeling of mixing in static mixers, Chem. Eng. Sci. 63 (2008) 4135–4149, http://dx.doi.org/10.1016/j.ces.2008.05.026.

[40] J.I. Langford, A.J.C. Wilson, Scherrer after sixty years: a survey and some new results in the determination of crystallite size, J. Appl. Crystallogr. 11 (1978) 102–113.

[41] D. Chiche, M. Digne, R. Revel, C. Chanéac, J.-P. Jolivet, Accurate determination of oxide nanoparticle size and shape based on X-ray powder pattern simulation: application to boehmite AlOOH, J. Phys. Chem. C 112 (2008) 8524–8533, http://dx.doi.org/10.1021/jp710664h.

[42] E.W. Washburn, Note on a method of determining the distribution of pore sizes in a porous material, Proc. Natl. Acad. Sci. 7 (1921) 115–116.

[43] K.S. Pitzer, Activity Coefficients in Electrolyte Solutions, second ed., CRC Press, 1991.

[44] K.S. Pitzer, Thermodynamics of electrolytes. I. Theoretical basis and general equations, J. Phys. Chem. 77 (1973) 268–277, http://dx.doi.org/10.1021/j100621a026.

[45] D.L. Parkhurst, C.A.J. Appelo, Description of input and examples for PHREEQC version 3 – a computer program for speciation, batch-reaction, one-dimensional transport, and inverse geochemical calculations, in: US Geol. Surv. Tech. Methods.

[46] J. Zhou, Q.Y. Chen, J. Li, Z.L. Yin, X. Zhou, P.M. Zhang, Isopiestic measurement of the osmotic and activity coefficients for the NaOH–$NaAl(OH)_4$–H_2O system at 313.2 K, Geochim. Cosmochim. Acta 67 (2003) 3459–3472, http://dx.doi.org/10.1016/S0016-7037(03)00133-9.

[47] C. Christov, A.G. Dickson, N. Moller, Thermodynamic modeling of aqueous aluminum chemistry and solid–liquid equilibria to high solution concentration and temperature. I. The acidic H–Al–Na–K–Cl–H_2O system from 0 to 100 °C, J. Solut. Chem. 36 (2007) 1495–1523, http://dx.doi.org/10.1007/s10953-007-9191-9.

[48] X. Li, L. Yan, Q. Zhou, G. Liu, Z. Peng, Thermodynamic model for equilibrium solubility of gibbsite in concentrated NaOH solutions, Trans. Nonferrous Met. Soc. China 22 (2012) 447–455, http://dx.doi.org/10.1016/S1003-6326(11)61197-7.

[49] J.-F. Boily, O. Qafoku, A.R. Felmy, A. Potentiometric, Spectrophotometric and Pitzer ion-interaction study of reaction equilibria in the aqueous H^+–Al^{3+}, H^+–oxalate and H^+–Al^{3+}–oxalate systems up to 5 mol dm^{-3} NaCl, J. Solut. Chem. 36 (2007) 1727–1743, http://dx.doi.org/10.1007/s10953-007-9203-9.

[50] W. Li, H. Muhr, E. Plasari, Use of different rapid mixing devices for controlling the properties of magnetite nanoparticles produced by precipitation, J. Cryst. Growth 342 (2012) 21–27, http://dx.doi.org/10.1016/j.jcrysgro.2011.05.031.

[51] R. Phillips, S. Rohani, J. Baldyga, Micromixing in a single-feed semi-batch precipitation process, AIChE J. 45 (1999) 82–92, http://dx.doi.org/10.1002/aic.690450108.